Nanoscale Advances

ROYAL SOCIETY OF CHEMISTRY

PAPER

View Article Online
View Journal | View Issue

Cite this: *Nanoscale Adv.*, 2020, **2**, 5219

Engineering the surface of graphene oxide with bovine serum albumin for improved biocompatibility in *Caenorhabditis elegans*†

S. Sivaselvam,[a] A. Mohankumar,[b] G. Thiruppathi,[b] P. Sundararaj,[b] C. Viswanathan[a] and N. Ponpandian*[a]

Graphene oxide (GO) has been extensively studied for its potential biomedical applications. However, its potential risk associated with the interactions of GO in a biological system hampers its biomedical applications. Therefore, there is an urgent need to enhance the biocompatibility of GO. In the present study, we decorated the surface of GO with bovine serum albumin (GO-BSA) to mitigate the *in vivo* toxic properties of GO. An *in vivo* model *Caenorhabditis elegans* has been used to study the potential protective effect of BSA decoration in mitigating GO induced toxicity. The BSA decoration on the surface of GO prevents the acute and prolonged toxicity induced by GO in primary and secondary organs by maintaining normal intestinal permeability, defecation behavior, development, and reproduction. Notably, GO-BSA treatment at 0.5–100 mg L^{-1} does not affect the intracellular redox status and lifespan of *C. elegans*. Reporter gene expression analysis revealed that exposure to GO-BSA (100 mg L^{-1}) did not significantly influence the nuclear accumulation and expression patterns of DAF-16/FOXO and SKN-1/Nrf2 transcription factors and their downstream target genes *sod-3, hsp-16.2, ctl-1,2,3, gcs-1,* and *gst-4* when compared to exposure to pristine GO. Also, quantitative real-time PCR results showed that GO-BSA did not alter the expression of genes involved in regulating DNA damage checkpoints (*cep-1, hus-1* and *egl-1*) and core signaling pathways of apoptosis (*ced-4, ced-3* and *ced-9*), in contrast to GO treatment. All these findings will have an impact on the future development of safer nanomaterial formulations of graphene and graphene-based materials for environmental and biomedical applications.

Received 13th July 2020
Accepted 12th September 2020

DOI: 10.1039/d0na00574f

rsc.li/nanoscale-advances

1. Introduction

Nanomaterials are unique materials that have turned out to be prominent in many fields, from electronics to energy storage applications. In recent years, graphene-based materials (GBMs) have expanded their application into medicine and life sciences. Among the GBMs, graphene oxide (GO) has been one of the most studied materials in the last decade due to its unique physico-chemical properties and potential multifunctional applications.[1] The unique properties of GO include high surface area, good biological stability and better dispersion in water due to its hydrophilic functional groups accumulated at the edges and basal plane of sheets.[2] Owing to its tunable characteristics, GO has turned out to be an excellent material in the biomedical field for drug delivery,[3] cellular imaging,[4] and bio-sensing.[5] Although the applications of GO advance the biomedical field, there are questions about the potential risks that it poses to environmental organisms and human health, raising safety concerns. Mounting preclinical studies suggest that exposure to GO produces adverse effects including the production of reactive oxygen species (ROS), induction of apoptosis, damage to DNA, development of thrombi, reproductive damage, and genotoxicity.[6–11] Earlier studies have also stated that the toxicity of GO, to a great extent, is due to its strong dispersion and the physical interaction between its surface and the cell membrane.[12,13] A detailed understanding of the nano-toxicity and the degree of toxicity that GO might achieve in a biological system is necessary for exploring the potential use of GO in biological applications.

Caenorhabditis elegans is a free-living soil nematode. A smaller size, constant cell number, translucent body, highly conserved genome, unique anatomical structure with a short lifespan, and ease of maintenance make *C. elegans* a highly informative and widely used animal model to study nanomaterial toxicity.[14] Moreover, several important biochemical and genetic pathways are conserved in *C. elegans*.[15] Its experimental potential provides an ideal system for exploring organism-specific questions in the *in vivo* model.[16] Previous studies confirmed that exposure of nematodes to GO could lead

[a]*Department of Nanoscience and Technology, Bharathiar University, Coimbatore 641 046, India. E-mail: ponpandian@buc.edu.in; Fax: +91-422-2422387; Tel: +91-422-2428421*

[b]*Department of Zoology, Bharathiar University, Coimbatore 641 046, India*

† Electronic supplementary information (ESI) available. See DOI: 10.1039/d0na00574f

to a lethal effect on their targeted organs.[16,17] Besides, oxidative stress, increased intestinal permeability, and damaged neuronal development are also responsible for GO induced toxicity in nematodes. Exposure to other nanomaterials including multi-walled carbon nanotubes, fullerenes, TiO_2, Ag, ZnO, SiO_2, Au, and iron oxide nanoparticles has also shown toxic effects in the nematode *C. elegans*.[18–23] Designing the surface of a nanomaterial is one of the key parameters in mitigating its toxicity to enhance its biocompatibility. The surface modification of superparamagnetic iron oxide nanoparticles with bovine serum albumin (BSA) reduced its toxicity in *C. elegans*.[24] The main problem with the use of GO in biology is its biocompatibility. Recently, surface coating of GO with fetal bovine serum (FBS) led to reduced toxicity in *C. elegans* when compared to that of pristine GO.[25,26] In recent years, it has become clear that the surface modification of GO improves its biocompatibility in *in vitro* and *in vivo* studies.[12,16] The surface modification of GO with polyethylene glycol (PEG) and carboxylic acid resulted in reduced toxicity in nematodes when compared with that of pristine GO.[27–29]

In the present study, an attempt has been made to develop a safe GO formulation and characterize its biological effects using *C. elegans*. It was hypothesized that decorating the surface of GO with bovine serum albumin (GO-BSA) can effectively reduce the toxicity of GO. However, the complete understanding of the *in vivo* behavior of GO-BSA remains largely unclear. Thus, we used the acute and prolonged assay method of *C. elegans* to analyze the protective effect of GO-BSA and compared the toxicity profiles of GO and GO-BSA. The current study provides a significant insight into the *in vivo* behavior of GO-BSA, which will have an impact on safer nanomaterial formulation and the biomedical application of graphene and graphene-based materials in the future.

2. Experimental section

2.1. Materials

Graphite (>20 μm), 2′,7′-dichlorofluorescein diacetate (H_2DCF-DA), 1-ethyl-3-(3-dimethylaminopropyl) carbodiimide (EDAC), bovine serum albumin (BSA) and Rhodamine-B were supplied by Sigma Aldrich. Sodium azide (NaN_3), 2-(*N*-morpholino) ethanesulfonic acid (MES), and Nile red dye were obtained from HiMedia Laboratories Pvt. Ltd., India. All other chemicals were purchased from Sigma Aldrich, India and used as received. Ultrapure water purified using a MilliQ (Millipore) system was used in all the experiments.

2.2. Preparation and purification of graphene oxide (GO)

GO sheets were prepared by a modified Hummers' method.[2] Briefly, graphite (2 g) and sodium nitrate (2 g) were taken in a 500 mL beaker, followed by the gradual addition of sulfuric acid (200 mL) while stirring with a magnetic stirrer and the temperature was maintained below 4 °C. Subsequently, 12 g of $KMnO_4$ was ground and progressively added to the mixture by controlling the temperature below 20 °C. Then, 185 mL of H_2O was gradually mixed into the above solution. Then, the temperature of the mixture was raised to 95 °C for 15 min and the mixture stirred for 2 h at 35 °C. Then, 10 mL of H_2O_2 (30%) was gradually added to reduce the unreacted potassium permanganate in the solution. The final precipitate was rinsed with 10 mL HCl (5%) and washed with deionized water until neutral pH was achieved, followed by drying under vacuum conditions at 65 °C for 12 h.

2.3. Decorating BSA on the surface of GO (GO-BSA)

BSA was chemically bonded to GO sheets by a two-stage process of diimide-activated amidation as described previously.[30] Briefly, a well-dispersed GO suspension of 100 mL (1 mg mL^{-1}) was taken. Then the above-mentioned suspension was rapidly blended with 50 mL of MES buffer (500 mM, pH 6.1) and 30 mL NHS solution (100 mg L^{-1}) for 30 min. The above solution was rapidly added and stirred continuously for 30 min with 60 mL of freshly prepared EDAC solution (10 mg L^{-1}). The above suspension was kept undisturbed for 2 h, followed by washing with MES buffer (50 mM) thoroughly to get rid of unbound NHS, EDAC, and the byproduct urea. The final sample was vacuum dried for 16 h at 50 °C.

In the second stage, the estered GO was dispersed in MES buffer (50 mM, pH 6.1) and stirred continuously for 30 min. Then, 10 mL of BSA (10 mg mL^{-1}) was added dropwise and the mixture kept in a shaker for 2 h at 150 rpm. The final solution was washed with MES buffer to remove the unbound BSA and dried at 50 °C for 16 h.

2.4. Maintenance of *C. elegans* and GO/GO-BSA exposure

The *C. elegans* strains used in this study were as follows: Bristol N2 (wild-type), TJ356 (*zIs356* [*daf-16::GFP*]), GA800 (*wuIs151* [*ctl-1,2,3::GFP*]), CF1553 (*muIs84* [*pAD76* (*sod-3::GFP*)]), LD1171 (*ldIs3* [*gcs-1::GFP*]), TJ375 (*gpls1* [*hsp-16.2::GFP*]), EG1285 (*oxIs12* [*unc-47::GFP*]), LD1 (*ldIs7* [*skn-1b/c::GFP*]), BZ555 (*egIs1* [*dat-1::GFP*]), CL2166 (*dvIs19* [*gst-4::GFP*]) and MD701 (*bcIs39* [*ced-1::GFP*]). All the strains were maintained and propagated at 20 °C on nematode growth medium (NGM) agar plates seeded with live *Escherichia coli* OP50 bacteria according to standard techniques.[31] Bleaching buffer solution was used to synchronize worms.[32] Working concentrations of 0.5–100 mg L^{-1} were prepared by diluting the stock solution of GO/GO-BSA (1 mg mL^{-1}). The acute exposure assay of GO/GO-BSA was carried out in L4 larva for 24 h and extended from the L1 larva stage to young adult for prolonged exposure assay in 24-well microtiter plates.

2.5. Reproduction and development

For the reproduction assay, worms (n = 20 worms per treatment) treated with GO/GO-BSA were transferred individually onto a fresh NGM plate every day, till the egg-laying capacity of worms reached zero. The number of offspring developed from eggs was recorded in the L3–L4 stage. The body sizes of the worms were studied to measure the growth of the worms. Briefly, 40 randomly chosen worms per treatment were analyzed using an Optika View image analysis system (Optika, Italy) for measuring the body length of the worms.[33] Three independent

biological trials were performed with appropriate replicates under similar conditions.

2.6. Lifespan analysis

About 30–40 age-sorted wild-type worms per experiment were treated with GO/GO-BSA at different concentrations ranging from 0.5 to 100 mg L^{-1}. Once the worms reached the L4 stage, they were moved to a new NGM plate spotted with 0.05 M 5-fluoro-2′-deoxyuridine (FUdR, Sigma) to inhibit the progeny development. Nematodes were periodically transferred to new plates to avoid contamination and starvation, followed by counting the number of living and dead worms on the plate. The worms exhibiting a bag of worms phenotype, mechanical death, and creeping movement off the plates were noted as censored. This assay was carried out until the last worm became censored. Three separate biological trials with four replicates were performed under the same conditions.[34]

2.7. Quantification of intestinal ROS production

To measure the production of intestinal ROS, GO/GO-BSA (0.5–100 mg L^{-1}) treated wild-type *C. elegans* (n = 25–30 worms per treatment) were shifted to a 24-well microtiter plate containing 1 mL of M9 buffer with 0.05 mM H_2DCF-DA. After 30 min incubation, the worms were washed with M9 buffer thrice. Then, 30 mM NaN_3 was used to anesthetize the worms which were mounted on a clean glass slide containing a 3% agar pad. The immobilized live worms were examined under laser scanning confocal microscopy (LSM 710, Zeiss, Germany), and ImageJ software was used to measure the intensity of DCF fluorescence.[35]

2.8. *In situ* bio-distribution of GO and GO-BSA in *C. elegans*

The *in vivo* bio-distribution of GO/GO-BSA inside the nematodes (n = 30–35 worms per experiment) was investigated by loading 300 μL of Rhodamine-B (2 mg mL^{-1}) on 10 mL of GO/GO-BSA (1 mg mL^{-1}) in the dark as previously described.[36] Then, the solution was dialyzed (10 000 MWCO) for 12 h with water for the removal of unbound Rhodamine B. The nematodes were treated with Rhodamine-B loaded GO/GO-BSA (100 mg L^{-1}) for 30 min and 3 h for acute and prolonged exposure, respectively, at 20 °C followed by washing and re-suspension in M9 buffer. The immobilized live worms were examined under laser scanning confocal microscopy, and the fluorescence intensity was measured as described above.

2.9. Defecation and locomotion behavior assay

GO/GO-BSA treated worms (n = 20–25 worms per experiment) were separated into a new NGM plate seeded with *E. coli* OP50. To analyze the mean defecation cycle length, the interval between two successive posterior body-wall muscles was recorded using an inverted microscope (XDS-2, Optika, Italy) for 2 min. For the analysis of locomotory behavior, the treated worms with GO/GO-BSA were subjected to analysis of head thrashes and body bends according to the methods described.[17]

2.10. Nile red staining

The effect of GO/GO-BSA (100 mg L^{-1}) on fat deposition can be examined in *C. elegans*; the treated worms (n = 20–25 worms per treatment) were collected in 1× PBS buffer and fixed for 2 min with 50% isopropanol. Then 150 μL of Nile red solution (stock solution: 0.5 mg Nile red in 1 mL acetone) was added, followed by incubation in the dark for 25 min and resuspension in M9 buffer. Then, 30 mM NaN_3 was used to immobilize the live worms which were mounted on a clean glass slide containing a 3% agar pad, followed by imaging with a confocal microscope.[37]

2.11. Assay for chemotaxis behavior

The chemotaxis behavior of *C. elegans* was examined following a method described previously.[38] Briefly, age-synchronized worms of the L1 stage (~200 worms per treatment) were exposed to GO/GO-BSA (100 mg mL^{-1}). The day-6 adult worms were relocated onto the chemotaxis plate, which was split into four identical quadrants (A_1, A_2, B_1, B_2). To parts A_1 and A_2 in the chemotaxis plate 10 μL of 1 M sodium acetate (attractant) was added on one side, and to the remaining two parts, B_1 and B_2, in the plate 10 μL of distilled water was added. The treated worms were placed in the middle of the chemotaxis plate, which was spotted with sodium azide (25 mM) on each side to paralyze the attracted worms.

The chemotaxis index (CI) was calculated after 90 min of incubation using the following equation:

$$\mathrm{CI} = (A_1 + A_2) - (B_1 - B_2)/N$$

where A_1 and A_2 represent the number of worms present in the attractant region, B_1 and B_2 represent the number of worms present in the control region, and N represents the total number of worms used for the assay.

2.12. Transgenic reporter assays

Worms expressing reporter GFP transgenes were treated with GO/GO-BSA at the indicated concentrations at 20 °C. After treatment, the GFP expressions in the worms were imaged using a confocal microscope. ImageJ software was used to quantify the GFP signals. Thirty worms were used for each experiment.[39]

2.13. Neuronal viability assay and food-sensing behavior

The transgenic *C. elegans* expressing the GFP reporter construct in dopaminergic neurons (*dat-1::GFP*; BZ555 strain) and D-type GABAergic motor neurons (*unc-47::GFP*; EG1285 strain) were used to study the neuronal health of nematodes exposed to GO and GO-BSA. Synchronized worms at the L3 stage (n = 20–25 worms per treatment) were exposed to GO/GO-BSA for 72 h. Then, the treated worms were washed with M9 buffer and imaged under a confocal microscope, and the neuronal health was measured by quantifying the GFP intensity. For the analysis of dopaminergic and GABAeric neuronal health, the GFP expressions in all eight dopaminergic neurons and the D-type GABAergic motor neurons were examined, respectively. The

effect of the dopaminergic neuron on slowing down the food response in *C. elegans* was evaluated by examining the food-sensing behavior. For the food-sensing assay, new NGM plates were prepared by spreading *E. coli* OP50 in a 9 cm diameter and incubating overnight at 37 °C as described earlier.[37] The examined nematodes were dropped in the middle of the NGM plate spotted with and without bacteria. After 5 min, the body bends of nematodes were measured for 60 s, and the slowing rate was determined as follows:

$$\text{Slowing rate} = (N_{\text{without food}} - N_{\text{with food}})/N_{\text{without food}}$$

where N represents the total number of body bends.

2.14. Analysis of germ cell apoptosis by CED-1 expression

To examine the effect of GO/GO-BSA on inducing germ cell apoptosis, a transgenic strain expressing the GFP reporter for *ced-1::GFP* (MD701) was used. Briefly, synchronized worms at the L3 stage (n = 30–40 worms per treatment) were exposed to GO/GO-BSA (100 mg mL^{-1}) for 72 h. After treatment, the fluorescence 'halo' pattern of *ced-1::GFP* on the engulfing sheath cells was quantified using a confocal microscope.[37]

2.15. Reverse-transcription and quantitative real-time polymerase chain reaction (qRT-PCR)

The total RNA from nematodes was extracted using TRIzol reagent (Invitrogen) according to the manufacturer's instructions. After RNA extraction, they were reverse transcribed using a RevertAid™ First-strand cDNA synthesis kit (Invitrogen). SYBR™ Green (Applied Biosystems™) was used to perform real-time qRT-PCR analysis to target the amplifying PCR product. The qRT-PCR was run at an optimized thermal profile as follows: 10 min at 95 °C, and 40 cycles of 15 s at 95 °C and 60 s at 60 °C. The final results are expressed as a fold change compared with reference gene act-1. The primer information for qRT-PCR is given in Table S2.†

2.16. Statistical analysis

Means of the treatment groups were compared with untreated control using a one-way analysis of variance (ANOVA) followed by a Bonferroni post hoc test using IBM SPSS 17.0 statistical software for Windows, v.17 (IBM Corporation, Armonk, NY, USA). Lifespan curves were plotted using the Kaplan–Meier survival method and analyzed by a log-rank test in MedCalc statistical tool, v.14 (MedCalc, Ostend, Belgium). Error bars indicate the mean value of three independent experimental datapoints, and probability levels of $p < 0.05$ were considered as statistically significant.

3. Results and discussion

3.1. Characterization of GO and GO-BSA

The preparation of bovine serum albumin decorated graphene oxide (GO-BSA) is schematically illustrated in Fig. S1.† The X-ray diffraction (XRD) pattern of GO in Fig. 1a shows a sharp diffraction peak at 10.3° which is assigned to the (001) plane of GO. In the XRD pattern of the GO-BSA composite, a broad and moderately strong peak is observed between 20 and 27°, attributed to the amide bond of BSA in GO-BSA. Meanwhile, the typical GO peak vanishes in the GO-BSA composite, and it could be due to the long-range disorder or full exfoliation of GO in the GO-BSA composite. Our results are in good agreement with previous reports.[40,41]

The successful formation of GO-BSA was further authenticated by Raman spectra as shown in Fig. 1b. In the GO spectrum, the D-band at 1352 cm^{-1} was attributed to the defect induced breathing mode of the sp^2 carbon ring, while the G-band at 1601 cm^{-1} was attributed to the E_{2g} phonon mode of the sp^2 C atom.[42] In the GO-BSA spectrum, the D-band (1353 cm^{-1}) and G-band (1607 cm^{-1}) are shifted to a higher wavelength that relates to the disturbance in the GO surface by the interaction between the carbon group of GO and amide group of BSA. Furthermore, the intensity ratio of the D and G bands (I_D/I_G) of GO is 1.09, and it is increased to 1.19 in GO-BSA. The increased intensity ratio (I_D/I_G) of GO-BSA indicates an increase in defect density, and it could be due to the exfoliation and chemical modification on GO. The shift in D and G bands and change in the intensity ratio of I_D/I_G indicates the attachment of BSA with GO.[43]

The functional groups present in the surface of GO and GO-BSA were examined by FTIR spectroscopy and the respective FTIR spectra are shown in Fig. 1c. In the FTIR spectrum of GO, a broad peak appears at 3430 cm^{-1} and is attributed to the stretching vibration of the O–H group. The absorption peak at 1600 cm^{-1} corresponds to the C=C stretching. The absorption peaks at 1739, 1242, and 1052 cm^{-1} belong to C=O, C–OH, and C–O stretching vibrations, respectively.[44] In the FTIR spectrum of protein BSA, the absorption peaks at 1646 and 1540 cm^{-1} correspond to the C=O stretching mode of amide I and N–H bending vibration of the amide II band, respectively. The absorption peak at 1384 cm^{-1} corresponds to the C–N stretching. The absorption peaks at 3435 and 2842 cm^{-1} correspond to the N–H and C–H stretching, respectively.[45] In the FTIR spectrum of GO-BSA, the absorption peak at 640 cm^{-1} corresponds to the O=C–NH in-plane vibration.[44] The absorption peak at 2845 cm^{-1} is attributed to the C–H stretching vibration of the methyl group in BSA. In addition, the appearance of a new band at 1680 cm^{-1} in the GO-BSA composite is due to the cross-linking of the carboxyl group in GO with the amide group of BSA to form an amide linkage.[44]

The UV-visible spectra of GO, BSA, and GO-BSA are shown in Fig. 1d. GO shows an absorption peak at 230 nm, which corresponds to the π–π* electron transition of the aromatic C–C bond, and the shoulder peak that appears at 310 nm represents the n–π* transition of the C=O group.[46] For pure BSA, two absorption peaks at 220 and 276 nm result from the backbone structure and aromatic amino acid present in BSA. Compared with GO, the absorption peak in the GO-BSA composite becomes sharpened and shifted to 279 nm, which is probably due to the strong interaction between GO and BSA.[47,48] The size distribution analysis by dynamic light scattering (DLS) shows that the average particle size distribution of GO is 164 nm, and the particle size increased to 180 nm after binding BSA with GO, which confirms the successful formation of GO-BSA (Fig. S2†). A

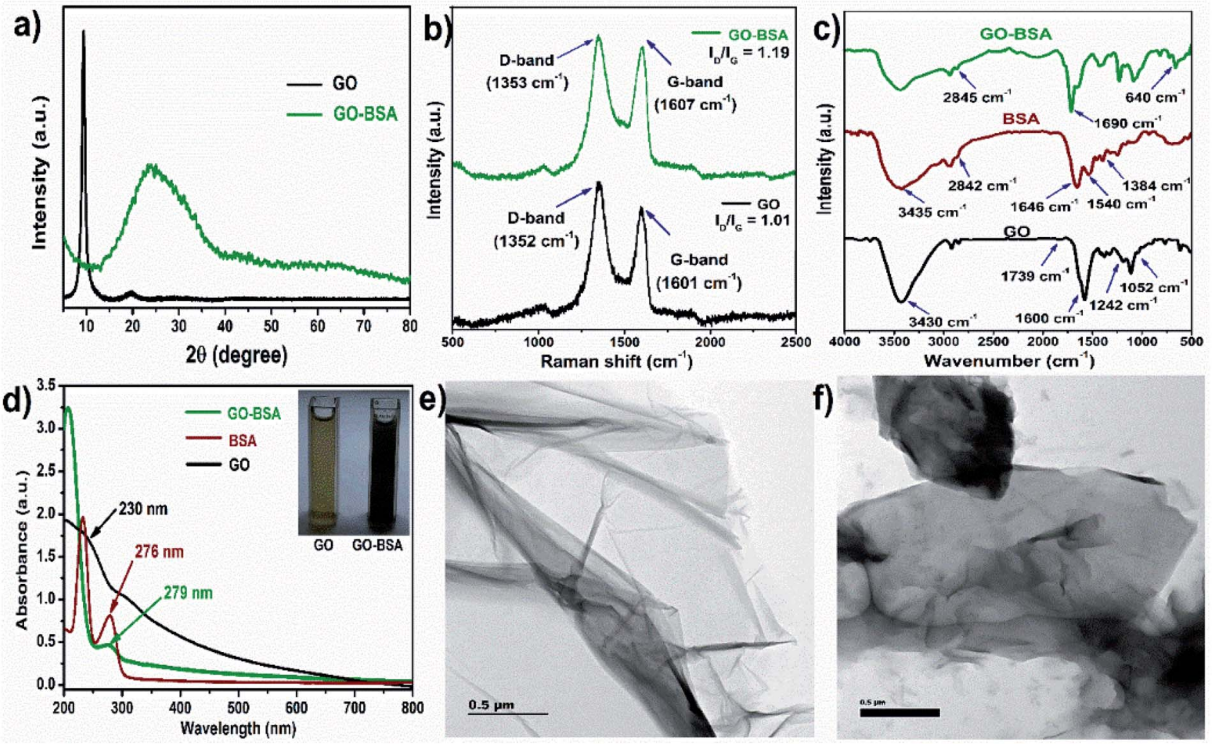

Fig. 1 Physicochemical properties of GO and GO-BSA. (a) XRD patterns, (b) Raman spectra, (c) FTIR spectra, (d) UV-visible spectra and TEM images of (e) GO and (f) GO-BSA.

transmission electron microscope (TEM) was employed to understand the microstructures of GO and GO-BSA. The TEM image of GO in Fig. 1e shows a transparent, smooth, and thin sheet-like structure. After surface decoration with BSA, Fig. 1f shows that the transparent sheet becomes dark and this could be due to the attachment of BSA on the GO sheet.[40] These results indicate the successful binding of BSA with the GO sheet.

3.2. Effect of acute exposure to GO/GO-BSA on wild-type nematodes

Mounting pre-clinical studies have shown that ENMs cause wild-type toxicity in *C.* elegans.[49–56] We first investigated the effect of acute exposure to GO/GO-BSA on wild-type N2 nematodes. Acute exposure to GO/GO-BSA (0.5–100 mg L−1) did not affect the normal lifespan as shown in Fig. S3a & b† and given in Table S1† or the development of nematodes as shown in Fig. 2a, at the studied concentrations. To determine the effect of GO and GO-BSA on the secondary targeted organs of nematodes, we measured the head thrashes, body bends, and brood size as endpoints, shown in Fig. 2b–d. Acute exposure to GO was found to significantly influence the function of secondary targeted organs by decreasing the locomotory behavior and brood size in nematodes only at higher concentrations (50–100 mg L^{-1}). In contrast, the secondary targeted organs of GO-BSA (0.5–100 mg L^{-1}) exposed nematodes were not significantly altered. These results suggest that BSA decorated GO (GO-BSA) did not induce a toxic effect at the indicated concentrations by retaining the regular physiological activities of nematodes. Furthermore, the impact of GO/GO-BSA on intestinal ROS production in nematodes has been studied (Fig. 3). This study found that the production of ROS in nematodes increased significantly with GO exposure (10–100 mg L^{-1}). In contrast, acute exposure to GO-BSA did not induce ROS generation in nematodes. From these results, it has been observed that the difference in the toxicological behavior of GO and GO-BSA could be due to their difference in physicochemical properties. Collectively, these data suggest that decorating the surface of GO with protein-like BSA potentially reduces its toxicity.

Translocation of nanomaterials into the targeted organs induces toxicity in nematodes.[15,36,56–58] Taking these facts into account, Rhodamine-B was loaded onto GO/GO-BSA to investigate its translocation inside the nematodes. Following acute exposure, GO (100 mg L^{-1}) was primarily expressed in the pharynx and intestine region of nematodes, and a noticeable amount of signal was observed in the secondary targeted organ of nematodes (Fig. S4†). In contrast, GO-BSA (100 mg L^{-1}) was translocated mainly in the head region near the pharynx, and a much less noticeable signal was observed in the targeted organs. In order to examine the effects of GO/GO-BSA on intestinal permeability, Nile red (fluorescent dye) was used to stain lipids in exposed nematodes, and acute GO (100 mg L^{-1}) exposure was found to increase the Nile red intensity in exposed nematodes significantly. In contrast, GO-BSA exposure (100 mg L^{-1}) did not drastically increase the Nile red intensity in exposed nematodes (Fig. S5†). These data show that BSA decorated GO (GO-BSA) did not affect the intestinal

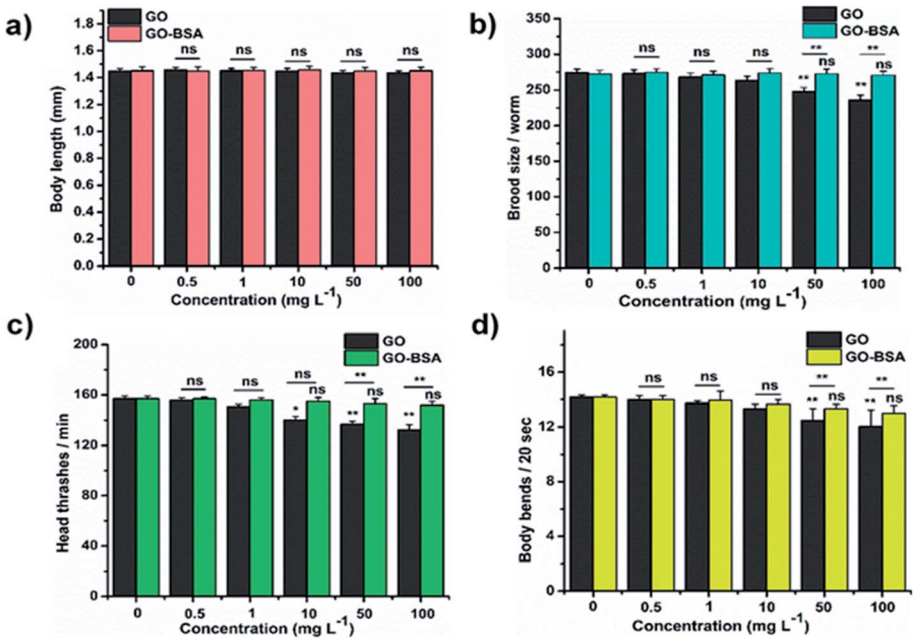

Fig. 2 Acute exposure assay of GO and GO-BSA on wild-type *C. elegans*. The effect of GO and GO-BSA on (a) body length, (b) brood size, (c) head thrashes, and (d) body bends. Error bars indicate the mean value of three independent experimental datapoints. $*p < 0.05$, $**p < 0.01$, and ns – not significant.

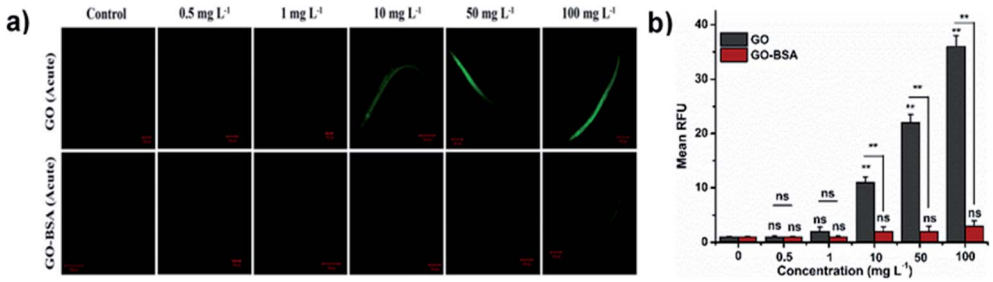

Fig. 3 Acute exposure assay of GO and GO-BSA on intestinal ROS production in wild-type *C. elegans*. (a) Fluorescent micrographs depicting the ROS production induced after acute exposure to GO and GO-BSA. (b) Quantification of DCF fluorescence in treated nematodes. Error bars indicate the mean value of three independent experimental datapoints ($n = 25$ per experiment). $**p < 0.01$, ns – not significant.

permeability and suppressed its translocation into secondary targeted organs when compared to GO exposed nematodes.

3.3. Physiological effects of prolonged exposure to GO and GO-BSA

The toxicity of ENMs in an environmental organism is mainly due to its long-term effect.[15] The effect of prolonged exposure to GO/GO-BSA on nematodes was investigated and it was found that exposure to 50–100 mg L^{-1} GO noticeably reduced the lifespan, as shown in Fig. S3(c & d) and Table S1.† Moreover, GO exposure (0.5–100 mg L^{-1}) significantly increased the intestinal ROS production (Fig. 5) and decreased the body length, brood size, and locomotory behavior of nematodes, as shown in Fig. 4. In contrast, prolonged exposure to GO-BSA at all tested concentrations did not alter the lifespan, body length, intracellular ROS levels, and reproduction & locomotion behaviors in nematodes. Therefore, our results indicate that prolonged exposure to GO-BSA does not interfere with the normal physiological function of primary and secondary targeted organs in nematodes. These data suggest that BSA decoration attenuates the GO-induced toxicity in the physiological function of nematodes.

3.4. BSA decoration alters the translocation pattern and intestinal permeability of GO

In *C. elegans*, translocation of ENMs into targeted organs could induce a lethal effect in nematodes.[15] The fluorescent probe Rhodamine-B was used to evaluate the translocation pattern of GO/GO-BSA (100 mg L^{-1}) in exposed nematodes. As a result, the GO-Rho-B signal was observed in both the primary and secondary targeted organs of the exposed nematodes (Fig. S6†). In contrast, the translocation pattern of GO-BSA was altered in the exposed nematodes when compared to GO. GO-BSA was expressed primarily in the pharynx, and the least amount of

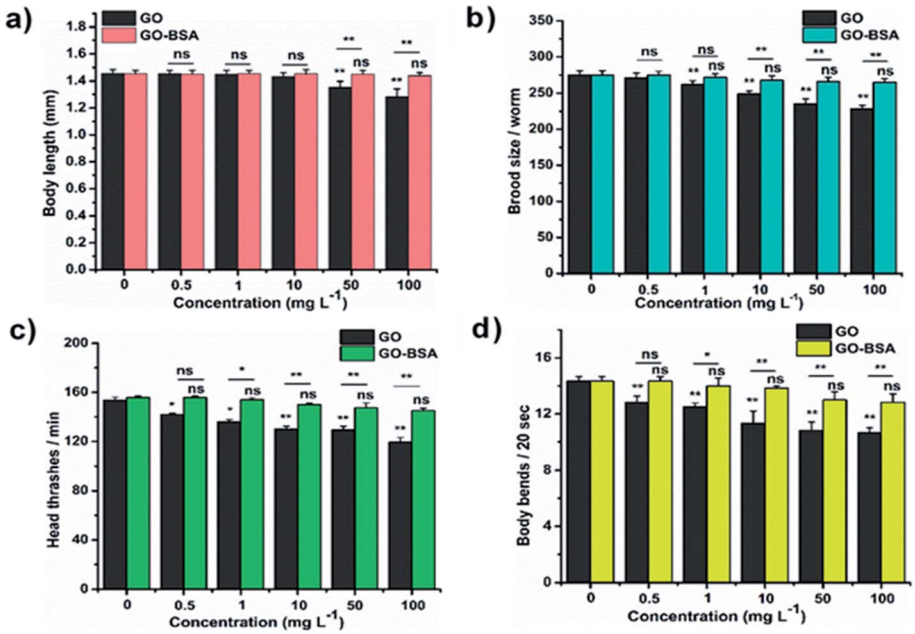

Fig. 4 Effect of prolonged exposure to GO and GO-BSA on *C. elegans* (N2 worms). The effect of GO and GO-BSA on (a) body length, (b) brood size, (c) head thrashes, and (d) body bends. Error bars indicate the mean value of three independent experimental datapoints ($n \geq 30$ per experiment). *$p < 0.05$, **$p < 0.01$, and ns – not significant.

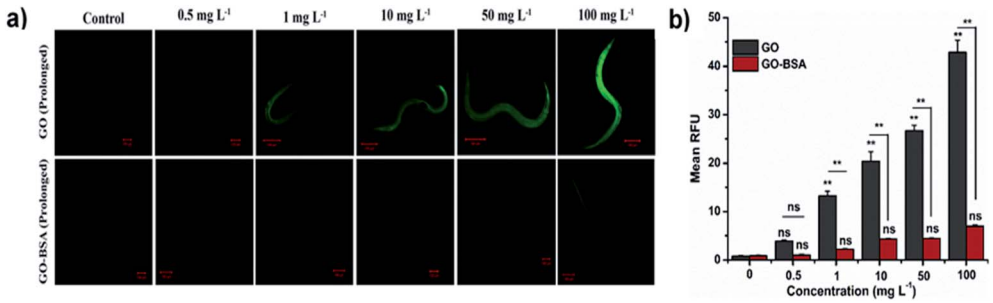

Fig. 5 Effect of prolonged exposure to GO and GO-BSA (100 mg L^{-1}) on intestinal ROS production in *C. elegans*. (a) Fluorescent micrographs depicting the ROS production after prolonged exposure to GO and GO-BSA. (b) Quantification of DCF fluorescence in treated nematodes. Error bars indicate the mean value of three independent experimental datapoints ($n = 25$ per experiment). **$p < 0.01$, ns – not significant.

signal was expressed in the intestine and secondary targeted organs of the exposed nematodes. Previous reports have shown that intestinal permeability may be responsible for the altered translocation pattern of ENMs.[15,57,58] The results indicate that GO exposure (100 mg L^{-1}) significantly increased the Nile red intensity in the intestine of nematodes, which shows severe damage in the intestinal barrier of exposed nematodes (Fig. S7†). In contrast, GO-BSA exposure did not significantly influence the lipid levels in nematodes. Our data suggest that BSA decoration significantly reduced the GO induced toxicity and its translocation into reproductive organs by maintaining the normal intestinal permeability in *C. elegans*.

3.5. BSA decorated GO maintains the normal defecation behavior

In *C. elegans*, alteration in defecation behavior by ENMs plays a crucial role in causing toxicity.[16,36] We next investigated the defecation behavior of nematodes exposed to GO/GO-BSA. Prolonged exposure to GO (1–100 mg L^{-1}) has significantly increased the defecation behavior in nematodes when compared to the control (Fig. 6a). However, GO exposure could not completely block the defecation behavior, and nematodes were able to remove a certain amount of GO. In contrast, GO-BSA exposure did not have a significant effect on the defecation behavior of nematodes. In *C. elegans*, the proper functioning of defecation behavior is controlled by AVL and DVB neurons.[59] Prolonged exposure to GO has significantly reduced the intensity of fluorescent puncta in AVL and DVB neurons when compared to the control (Fig. 6b). In contrast, fluorescent puncta of AVL and DVB neurons remained unchanged in BZ555 nematodes exposed to GO-BSA. These data further imply that surface decoration of GO with BSA might limit its entry into secondary targeted organs by maintaining the normal defecation cycle.

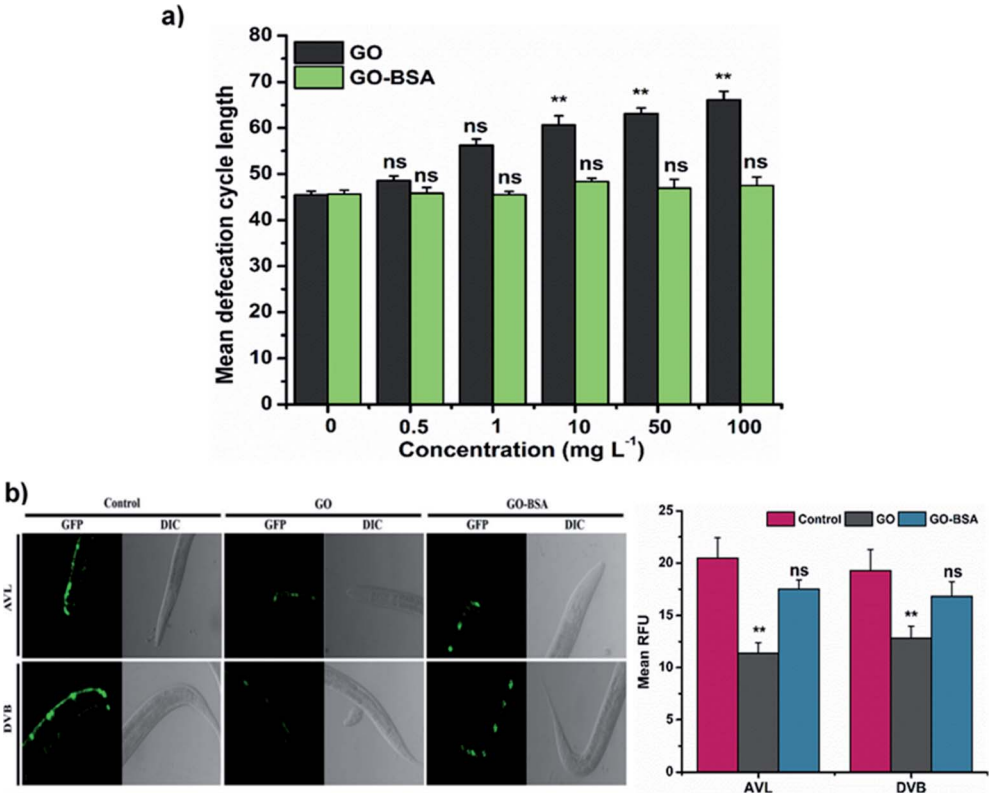

Fig. 6 Effect of GO and GO-BSA (100 mg L^{-1}) on defecation behavior in wild-type *C. elegans*. (a) Effect of GO and GO-BSA on defecation length in *C. elegans*. (b) Fluorescence micrographs showing the effect of GO and GO-BSA on the development of AVL and DVB neurons. Quantification of relative fluorescent puncta of AVL and DVB neurons after prolonged exposure to GO and GO-BSA. Error bars indicate the mean value of three independent experimental datapoints ($n \geq 30$ per experiment). $^{**}p < 0.01$, ns – not significant.

3.6. GO-BSA does not alter the development and functional status of neurons

The proper functional state of neurons is required to protect nematodes from toxicants.[60] To investigate the effect of GO/GO-BSA (100 mg L^{-1}) on the development and function of neurons, we used a *C. elegans* strain carrying the GFP transgene construct tagged in GABAergic and DAergic neurons. After GO-BSA exposure, no significant changes in GFP expression were observed in GABAergic and DAergic neurons. In contrast, GFP intensity in all eight DAergic neurons was decreased by about 55% in nematodes exposed to GO. Similarly, we observed significantly reduced fluorescent puncta, neuronal loss, and formation of damaged neurons on both the dorsal and ventral cords of the GABAergic motor neuron (Fig. 7a). We also investigated the effect of GO/GO-BSA on neurons, chemotaxis, and food searching behavior. It was observed that wild-type worms exposed to GO-BSA did not affect chemotaxis and food sensing behavior, which indicated the healthy status of neurons (Fig. 7b and c). Nematodes treated with GO alone significantly reduced the chemotaxis and food sensing behavior when compared to the control. From the above results, it was apparent that BSA decoration strikingly attenuated the GO-induced damage on neuronal development and maintained the functional state of the neurons.

3.7. Effects of GO and GO-BSA on the oxidative stress response mechanism

In *C. elegans*, the intracellular ROS production triggers several genes involved in the detoxification mechanism.[59] Therefore, the effects of GO/GO-BSA on key stress-responsive genes were studied. In nematodes, DAF-16/FOXO, and SKN-1/Nrf2 transcription factors confer stress resistance *via* regulating the expression of conserved antioxidant genes.[35] The results indicated that GO triggered the constitutive nuclear localization of *daf-16::GFP* and *skn-1b/c::GFP*, while GO-BSA did not influence the nuclear localization when compared to the control (Fig. S8†). We next investigated the expression pattern of the downstream targets of DAF-16 and SKN-1 transcription factors (Fig. 8). As a result, GO exposure significantly increased the expression levels of DAF-16 targets *sod-3::GFP*, *hsp-16.2::GFP* and *ctl-1,2,3::GFP*, and SKN-1 target genes *gst-4::GFP* and *gcs-1::GFP*. Conversely, no significant alteration in the expression levels of genes involved in DAF-16 and SKN-1 transcription factors was found in GO-BSA exposed nematodes when compared to the control. These data further confirm that the BSA decoration mitigates the GO induced toxicity in nematodes.

3.8. GO-BSA did not induce germline cell apoptosis in *C. elegans*

To study the effect of GO/GO-BSA (100 mg L^{-1}) on the induction of germline apoptosis in *C. elegans*, the MD701 strain carrying

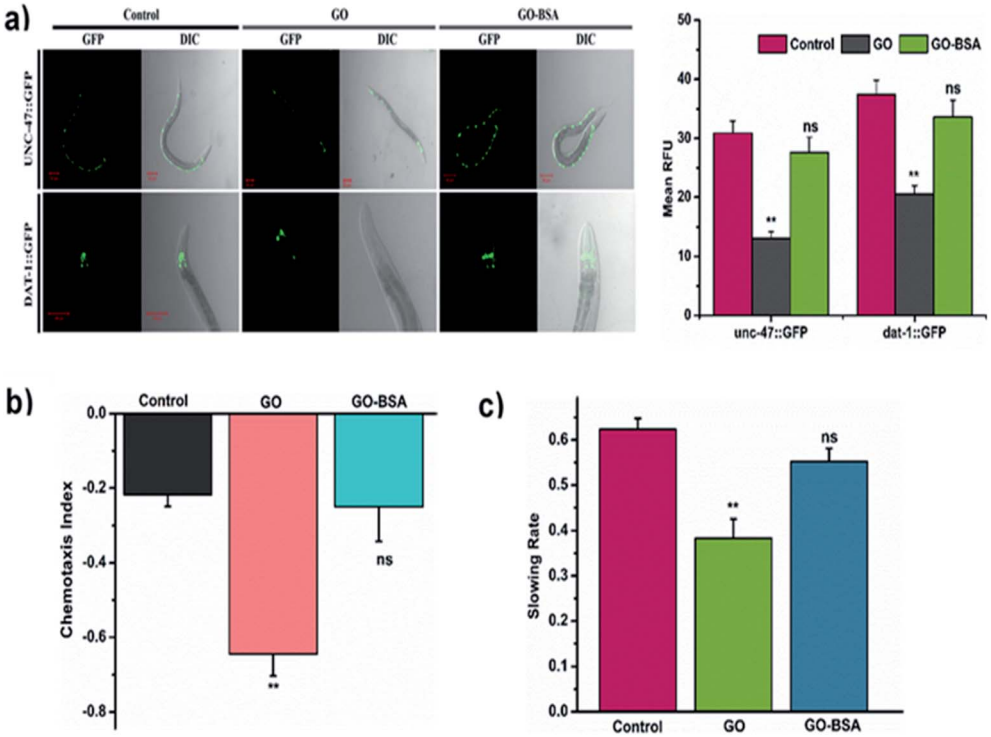

Fig. 7 Effect of GO and GO-BSA (100 mg L^{-1}) on the development of neurons in *C. elegans*. (a) The respective fluorescent images depict the GFP expression pattern of *unc-47::GFP* and *dat-1::GFP* transgene worms treated with GO and GO-BSA. (b) Comparison of chemotaxis and (c) food searching behavior in *C. elegans* after prolonged exposure. Error bars indicate the mean value of three independent experimental datapoints (n = 20 per experiment). **p < 0.01, ns – not significant.

CED-1::GFP fusion protein was used. As a result, GO exposure significantly increased the expression of CED-1::GFP clusters around cell corpses, while GO-BSA did not induce such expression in MD701 nematodes (Fig. 9a). This result shows that surface decoration of BSA with GO did not induce apoptosis in nematodes when compared to GO. Previous studies have

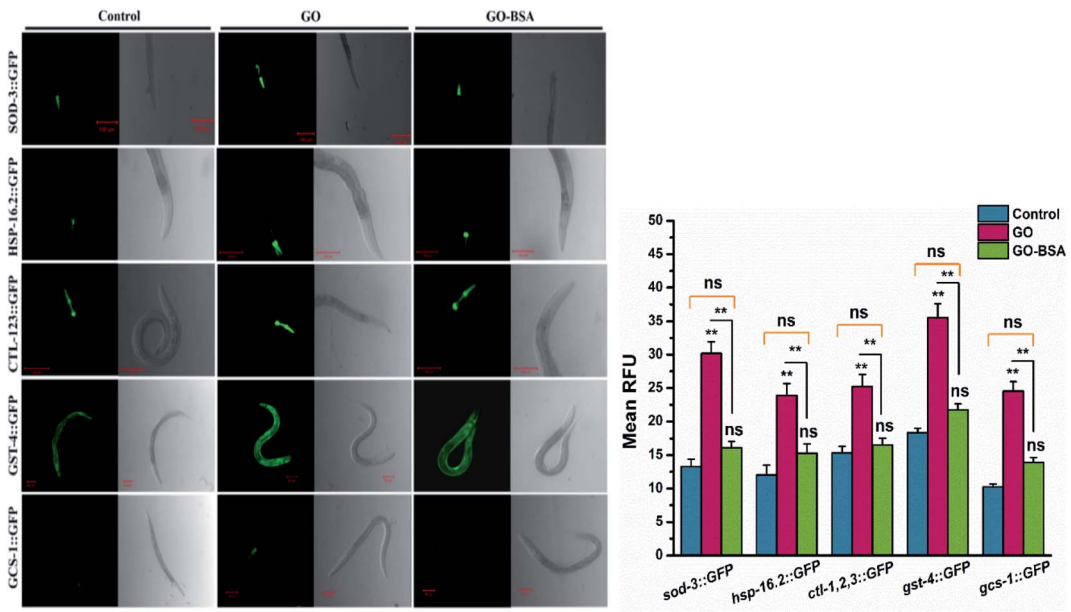

Fig. 8 Effect of GO and GO-BSA (100 mg L^{-1}) on the expression of antioxidant defense genes in *C. elegans*. Representative fluorescent images showing the expression of *sod-3*::GFP, *hsp-16.2*::GFP, *ctl-1,2,3*::GFP, *gst-4*::GFP and *gcs-1*::GFP and its quantified expression rate after prolonged exposure to GO and GO-BSA. Error bars indicate the mean value of three independent experimental datapoints (n = 20 per experiment). **p < 0.01, ns – not significant.

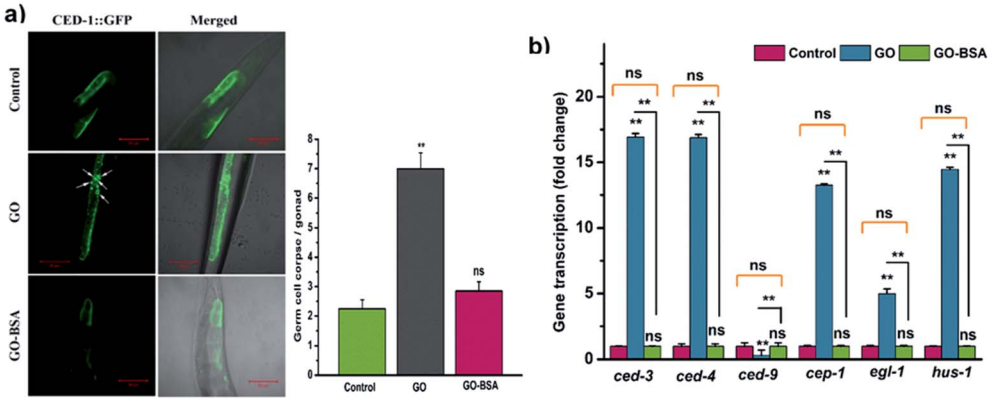

Fig. 9 Effect of GO and GO-BSA (100 mg L^{-1}) on the induction of germline apoptosis. (a) Representative images depicting the effect of GO and GO-BSA on the induction of germline apoptosis using the *ced-1::GFP* transgene in the MD701 strain, and their respective micrographs showing the number of apoptotic cells in the gonad arm. The arrowhead represents the apoptotic cells in the gonad. (b) Expression patterns of genes required for control of apoptosis and DNA damage in nematodes exposed to GO and GO-BSA with the untreated control using qRT-PCR. Error bars indicate the mean value of three independent experimental datapoints ($n = 20$ per experiment). $^{**}p < 0.01$, ns – not significant.

confirmed that GO exposure induces germline cell apoptosis by regulating the core components of apoptotic machinery genes *ced-9*, *ced-4*, and *ced-3*.[61] In *C. elegans*, CED-4 and CED-3 are homologous to mammalian Apaf-1 and caspase protein, respectively, which are required for the execution of apoptosis. CED-9, a Bcl-2 homologous protein, negatively regulates Apaf-1 like protein CED-4, which activates the CED-3 caspase to promote apoptosis. The gene expression analysis by qRT-PCR showed that GO-BSA exposure did not alter the expression rate of *ced-9*, *ced-4* and *ced-3* genes, while GO exposure upregulated *ced-4* and *ced-3* genes to 16 fold, and downregulated *ced-9* expression by 0.3 fold (Fig. 9b). In addition, the prolonged exposure to GO significantly increased the expression of genes involved in oxidative stress-induced DNA damage like *hus-1*, *cep-1*, and *egl-1* genes when compared to the control. These results are consistent with the earlier observation.[17] The activation of HUS-1 could further activate the DNA damage signaling pathway through CEP-1 and EGL-1.[61] EGL-1 is a pro-apoptotic BH-3 domain which inhibits the function of CED-9. CEP-1 is an ortholog of mammalian p53 which promotes DNA-damage induced apoptotic cell death by positively regulating EGL-1. Interestingly, GO-BSA did not cause any significant difference in the expression pattern of genes involved in germline cell apoptosis and DNA-damage induced apoptosis, as reflected by the gene expression analysis. These data confirm that BSA decoration mitigates GO-induced DNA damage and germline cell apoptosis.

4. Conclusion

In conclusion, to mitigate the toxic effect of GO, we have decorated its surface with BSA and investigated its *in vivo* effect using *C. elegans* as an animal model. It was observed that the prolonged GO-BSA exposure did not affect the function of primary and secondary targeted organs. In addition, the GO-BSA did not affect the normal intestinal permeability and defecation behavior in nematodes when compared to GO. The synergetic effect of intestinal permeability and defecation behavior in GO-BSA treated nematodes mitigates its translocation into secondary targeted organs. Furthermore, the GO-BSA did not affect the functioning of neurons and the antioxidant defense system in *C. elegans* when compared to GO. Besides, the expression levels of genes involved in germline cell apoptosis and DNA damage-induced apoptosis were not altered by GO-BSA. We conclude that the normal functioning of intestinal barriers, defecation behavior, neuronal health, and the antioxidant defense system in GO-BSA exposed nematodes greatly contribute to its non-toxic properties. Our results provide insight into the future development of safer nanomaterial formulations, thus facilitating their growing use in environmental and biomedical applications.

Conflicts of interest

There are no conflicts to declare.

Acknowledgements

We would like to thank the DST-FIST, DST-PURSE and UGC-SAP, Government of India, for the instrumentation facilities available at the Department of Nanoscience and Technology, Bharathiar University, India. The authors gratefully acknowledge the Caenorhabditis Genetic Centre (CGC, Universityof Minnesota, MN, USA), which is funded by the NIH Office of Research Infrastructure Programs (P40 OD010440), for providing *C. elegan* strains, and Bharathidasan University for the Confocal Laser Scanning Microscopy facility created through DST-PURSE, Govt. of India (Ref. No. SR/FT/LS-113/2009). A special thanks to Prof. R. Sathishkumar and Mrs. G. Mohanapriya, Department of Biotechnology, Bharathiar University, for their suggestions during the work. We also thank the DST FIST (SR/FST/LS-I/2017/10) supported department of Microbial Biotechnology, Bharathiar University, for providing the common instrumentation facility necessary for this work.

One of the authors, SS, would like to thank Bharathiar University for the University Research Fellowship (Ref. No. C2/7739/2019).

References

1 S. Das, S. Mitra, S. M. P. Khurana and N. Debnath, *Front. Life Sci.*, 2013, **7**, 90–98.
2 W. S. Hummers and R. E. Offeman, *J. Am. Chem. Soc.*, 1958, **80**, 1339.
3 G. Bharath, B. S. Latha, E. H. Alsharaeh, P. Prakash and N. Ponpandian, *Anal. Methods*, 2017, **9**, 240–252.
4 X. Sun, Z. Liu, K. Welsher, J. T. Robinson, A. Goodwin, S. Zaric and H. Dai, *Nano Res.*, 2008, **1**, 203–212.
5 H. Chang, L. Tang, Y. Wang, J. Jiang and J. Li, *Anal. Chem.*, 2010, **82**, 2341–2346.
6 O. Akhavan, E. Ghaderi and A. Akhavan, *Biomaterials*, 2012, **33**, 8017–8025.
7 N. Chatterjee, H. J. Eom and J. Choi, *Biomaterials*, 2014, **35**, 1109–1127.
8 M. C. Duch, G. R. S. Budinger, Y. T. Liang, S. Soberanes, D. Urich, S. E. Chiarella, L. A. Campochiaro, A. Gonzalez, N. S. Chandel, M. C. Hersam and G. M. Mutlu, *Nano Lett.*, 2011, **11**, 5201–5207.
9 M. U. Farid, S. Jeong, D. H. Seo, R. Ahmed, C. Lau, N. K. Gali, Z. Ning and A. K. An, *Nanoscale*, 2018, 4475–4487.
10 C. Fu, T. Liu, L. Li, H. Liu, Q. Liang and X. Meng, *Biomaterials*, 2015, **40**, 23–31.
11 A. B. Seabra, A. J. Paula, R. De Lima, O. L. Alves and N. Durán, *Chem. Res. Toxicol.*, 2014, **27**, 159–168.
12 G. Duan, S. Kang, X. Tian, J. A. Garate, L. Zhao, C. Ge and R. Zhou, *Nanoscale*, 2015, **7**, 15214–15224.
13 Y. Tu, M. Lv, P. Xiu, T. Huynh, M. Zhang, M. Castelli, Z. Liu, Q. Huang, C. Fan, H. Fang and R. Zhou, *Nat. Nanotechnol.*, 2013, **8**, 594–601.
14 L. Gonzalez-Moragas, L. L. Maurer, V. M. Harms, J. N. Meyer, A. Laromaine and A. Roig, *Mater. Horiz.*, 2017, **4**, 719–746.
15 Q. Wu, L. Yin, X. Li, M. Tang, T. Zhang and D. Wang, *Nanoscale*, 2013, **5**, 9934.
16 Y. Zhao, X. Yu, R. Jia, R. Yang, Q. Rui and D. Wang, *Sci. Rep.*, 2015, **5**, 1–13.
17 Q. Wu, Y. Zhao, Y. Li and D. Wang, *Nanoscale*, 2014, **6**, 11204–11212.
18 Q. Wu, A. Nouara, Y. Li, M. Zhang, W. Wang, M. Tang, B. Ye, J. Ding and D. Wang, *Chemosphere*, 2013, **90**, 1123–1131.
19 L. Gonzalez-Moragas, S. M. Yu, N. Benseny-Cases, S. Stürzenbaum, A. Roig and A. Laromaine, *Nanotoxicology*, 2017, **11**, 647–657.
20 M. Walczynska, W. Jakubowski, T. Wasiak, K. Kadziola, N. Bartoszek, S. Kotarba, M. Siatkowska, P. Komorowski and B. Walkowiak, *Toxicol. Mech. Methods*, 2018, **28**, 432–439.
21 C. C. Hu, G. H. Wu, S. F. Lai, M. Muthaiyan Shanmugam, Y. Hwu, O. I. Wagner and T. J. Yen, *Sci. Rep.*, 2018, **8**, 1–10.
22 J. Moon, J. Il Kwak and Y. An, *Chemosphere*, 2019, **215**, 50–56.
23 Y. J. Cha, J. Lee and S. S. Choi, *Chemosphere*, 2012, **87**, 49–54.
24 L. Gonzalez-Moragas, S.-M. Yu, E. Carenza, A. Laromaine and A. Roig, *ACS Biomater. Sci. Eng.*, 2015, **1**, 1129–1138.
25 Q. Wu, X. Zhou, X. Han, Y. Zhuo, S. Zhu, Y. Zhao and D. Wang, *Biomaterials*, 2016, **102**, 277–291.
26 G. Xiao, L. Zhi, X. Ding, Q. Rui and D. Wang, *RSC Adv.*, 2017, **7**, 52694–52701.
27 K. Yang, Y. Li, X. Tan, R. Peng and Z. Liu, *Small*, 2013, **9**, 1492–1503.
28 Q. Wu, Y. Zhao, J. Fang and D. Wang, *Nanoscale*, 2014, **6**, 5894.
29 J. Yang, Y. Zhao, Y. Wang, H. Wang and D. Wang, *Toxicol. Res.*, 2015, **4**, 1498–1510.
30 J. Shen, M. Shi, B. Yan, H. Ma, N. Li, Y. Hu and M. Ye, *Colloids Surf., B*, 2010, **81**, 434–438.
31 S. Brenner, *Genetics*, 1974, **77**, 71–94.
32 V. Singh, K. S. Rawat, S. Mishra, T. Baghel, S. Fatima, A. A. John, N. Kalleti, D. Singh, A. Nazir, S. K. Rath and A. Goel, *J. Mater. Chem. B*, 2018, **6**, 3366–3371.
33 S. Govindan, M. Amirthalingam, K. Duraisamy, T. Govindhan, N. Sundararaj and S. Palanisamy, *Biomed. Pharmacother.*, 2018, **102**, 812–822.
34 G. Devagi, A. Mohankumar, G. Shanmugam, S. Nivitha, F. Dallemer, P. Kalaivani, P. Sundararaj and R. Prabhakaran, *Sci. Rep.*, 2018, **8**, 7688.
35 A. Mohankumar, G. Devagi, G. Shanmugam, S. Nivitha, P. Sundararaj, F. Dallemer, P. Kalaivani and R. Prabhakaran, *Eur. J. Med. Chem.*, 2019, **168**, 123–133.
36 L. Zhi, M. Ren, M. Qu, H. Zhang and D. Wang, *Sci. Rep.*, 2016, **6**, 1–10.
37 A. Mohankumar, G. Shanmugam, D. Kalaiselvi, C. Levenson, S. Nivitha, G. Thiruppathi and P. Sundararaj, *RSC Adv.*, 2018, **8**, 33753–33774.
38 C. I. Bargmann, *Science*, 1998, **282**, 2028–2033.
39 G. Shanmugam, A. Mohankumar, D. Kalaiselvi, S. Nivitha, E. Murugesh, P. Shanmughavel and P. Sundararaj, *Biomed. Pharmacother.*, 2017, **95**, 1693–1703.
40 X. Yu, S. Sun, L. Zhou, Z. Miao, X. Zhang, Z. Su and G. Wei, *Nanomaterials*, 2019, **9**, 276.
41 P. Yang, Q. Liu, J. Liu, H. Zhang, Z. Li, R. Li, L. Liu and J. Wang, *Ind. Eng. Chem. Res.*, 2017, **56**, 3588–3598.
42 S. Chen, Q. Jiang, Y. Chen, L. Feng and D. Wu, *Nanomaterials*, 2019, **9**, 628.
43 M. Li, Y. Wang, Q. Liu, Q. Li, Y. Cheng, Y. Zheng, T. Xi and S. Wei, *J. Mater. Chem. B*, 2013, **1**, 475–484.
44 P. Yang, Q. Liu, J. Liu, H. Zhang, Z. Li, R. Li, L. Liu and J. Wang, *Ind. Eng. Chem. Res.*, 2017, **56**, 3588–3598.
45 A. Retnakumari, S. Setua, D. Menon, P. Ravindran, H. Muhammed, T. Pradeep, S. Nair and M. Koyakutty, *Nanotechnology*, 2010, **21**, 055103.
46 C. H. Manoratne, S. R. D. Rosa and I. R. M. Kottegoda, *Mater. Sci. Res. India*, 2017, **14**, 19–30.
47 H. Xu, N. Yao, H. Xu, T. Wang, G. Li and Z. Li, *Int. J. Mol. Sci.*, 2013, **14**, 14185–14203.
48 J. Shen, B. Yan, M. Shi, H. Ma, N. Li and M. Ye, *J. Colloid Interface Sci.*, 2011, **356**, 543–549.
49 S.-K. Jung, X. Qu, B. Aleman-Meza, T. Wang, C. Riepe, Z. Liu, Q. Li and W. Zhong, *Environ. Sci. Technol.*, 2015, **49**, 2477–2485.

50 S. Bosch, T. L. Botha, A. Jordaan, M. Maboeta and V. Wepener, *J. Toxicol.*, 2018, **2018**, 1–11.
51 A. Scharf, A. Piechulek and A. von Mikecz, *ACS Nano*, 2013, **7**, 10695–10703.
52 X. Yang, A. P. Gondikas, S. M. Marinakos, M. Auffan, J. Liu, H. Hsu-Kim and J. N. Meyer, *Environ. Sci. Technol.*, 2012, **46**, 1119–1127.
53 S. Rogers, K. M. Rice, N. D. Manne, T. Shokuhfar, K. He, V. Selvaraj and E. R. Blough, *SAGE Open Med.*, 2015, **3**, 205031211557538.
54 L. Zhao, H. Wan, Q. Liu and D. Wang, *Part. Fibre Toxicol.*, 2017, **14**, 27.
55 Y.-F. Yang, Y.-J. Lin and C.-M. Liao, *Int. J. Nanomed.*, 2017, **12**, 4607–4621.
56 M. Ren, L. Zhao, X. Ding, N. Krasteva, Q. Rui and D. Wang, *Part. Fibre Toxicol.*, 2018, 1–16.
57 Q. Wu, Y. Li, Y. Li, Y. Zhao, L. Ge, H. Wang and D. Wang, *Nanoscale*, 2013, **5**, 11166.
58 D. Wang, *Toxicol. Res.*, 2016, **5**, 1003–1011.
59 J. Yang, Y. Zhao, Y. Wang, H. Wang and D. Wang, *Toxicol. Res.*, 2015, **4**, 1498–1510.
60 Y. Zhao, X. Wang, Q. Wu, Y. Li, M. Tang and D. Wang, *Toxicol. Res.*, 2015, **4**, 399–408.
61 Y. Zhao, Q. Wu and D. Wang, *Biomaterials*, 2016, **79**, 15–24.

